RANGE AZIMUTH INDICATION USING A RANDOM FREQUENCY DIVERSE ARRAY

Yimin Liu

Department of Electronic Engineering
Tsinghua University
yiminliu@tsinghua.edu.cn

ABSTRACT

In this paper, a new type of antenna array, termed the Random Frequency Diverse Array (RFDA), is proposed to determine the target range and azimuth with low system complexity. Each antenna in the array has a narrow bandwidth and a randomly assigned carrier frequency. The beampattern of the RFDA is thumbtack-like. Moreover, the new approach can be considered a random sampling of target information in the spatial-frequency domain, which coincides with the basic concept of compressive sensing. With sparse recovery algorithms, the RFDA can detect the targets and successfully estimate their range and azimuth. The performance of this new approach is verified with numerical results.

***Index Terms*—** Wideband antenna array, compressive sensing, range azimuth estimation.

1. INTRODUCTION

Antenna arrays are quite popular in active sensing, for example, in radar, sonar, and ultrasonic technologies [1]. Using an antenna array, the beam can be flexibly steered, and the target direction can be effectively identified. In most target-locating applications, not only the direction but also the target range is important [2]. High-accuracy range indication requires that the signal transmitted and received by the array covers a sufficiently wide bandwidth. However, most array-processing theories and methods are based on the narrow-band assumption, and the wide signal bandwidth creates difficulties for signal processing and increases the system complexity [3].

Recently, the Frequency Diverse Array (FDA) technique [4] has been introduced. By linearly shifting the carrier frequencies across the array, the FDA can achieve a beampattern that depends on both the range and azimuth, and maintain a narrow bandwidth for each antenna. However, the range and azimuth are coupled [4].

In this paper, a new type of antenna array, named the Random Frequency Diverse Array (RFDA), is proposed to obtain the decoupled target range and azimuth. In the RFDA, the transceivers of every antenna remain narrowband, but their carrier frequencies are randomly arranged. It is shown that the beampattern of the RFDA is thumbtack-like, which implies that the range and azimuth are decoupled. Furthermore, with sparse recovery algorithms, the RFDA can detect multiple targets and successfully determine their ranges and azimuths. The numerical results for both single- and multiple-snapshot cases are presented to demonstrate the efficiency of the RFDA.

***Relation to prior work*:** To overcome the range-azimuth coupling in FDA, many methods, such as MIMO [5, 6], subarray [7], and double pulse [8] methods, have been introduced. However, these methods increase the system complexity [5, 6, 7] or the observation time [8]. In the present study, we regard the wideband antenna array as a sampling approach for target information in the spatial-frequency domain, and then formulate a random and sparse sampling scheme through randomly assigning the carrier frequencies of antennas. The corresponding mutual coherence [9] of the observing matrix is remarkably small, which complies with the requirement of compressive sensing. So a good performance without increasing the transceivers' bandwidth and system complexity can be expected.

The remainder of this paper is organized as follows. In Section 2, the system sketch is given, and the signal model is constructed. The beampattern of the RFDA is derived in Section 3. The target range and azimuth indication for both single- and multiple-snapshot cases are formulated as sparse recovery problems in Section 4. The numerical demonstrations are provided in Section 5. Conclusions are drawn in the final section.

2. SYSTEM SKETCH AND SIGNAL MODEL

Fig. 1 shows a cutline of the system sketch and target scenario of the RFDA.

In the RFDA, N antennas are located symmetrically along the x-axis at a constant inter-element distance d. The location x_n of the nth antenna is then

$$x_n = \left(-\frac{N-1}{2} + n\right) d, n = 0, 1, \ldots, N-1. \qquad (1)$$

Each antenna is connected with a narrow-band transceiver.

Project 61201356 and 61571260 supported by National Natural Science Foundation of China.

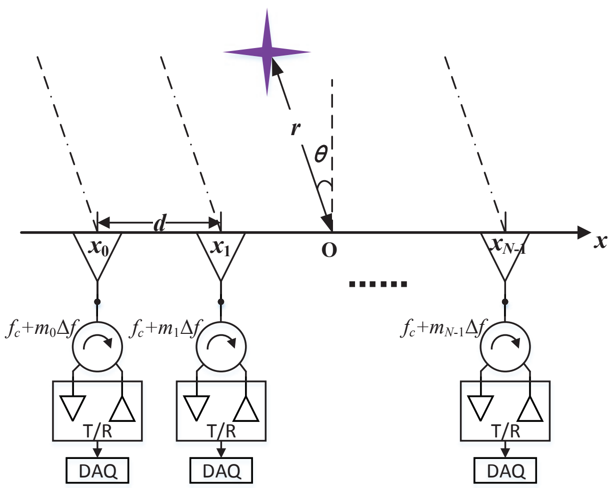

Fig. 1. System sketch and target scenario of the RFDA.

In the RFDA, the carrier frequency of the transceiver is randomly assigned as

$$f_n = f_c + m_n \Delta f, \tag{2}$$

where f_c is the center frequency of the array, Δf is the frequency increment step, and m_n is a random variable. In this paper, m_n are chosen to be independent identically distributed (*i.i.d.*), and $m_n \sim g(m_n)$, where $g(m_n)$ is the probability density function. The interval of m_n in which $g(m_n) \neq 0$ is determined as the entire bandwidth of the array. The origin of the x-axis is the phase center of the array. With this definition, the transmitted waveform of the nth antenna is

$$s_n(t) = e^{j2\pi(f_c+m_n\Delta f)t}. \tag{3}$$

For one ideal unit point target at range r and azimuth θ, with the far-field assumption, the received echo of the nth antenna is

$$r_n(t; r, \theta) = s_n(t - 2\frac{r + x_n \sin\theta}{c}) \tag{4}$$

where c is the speed of light. If we demodulate the received echo with the transmitted waveform and substitute (1) into (4), the baseband echo is

$$\begin{aligned} b_n(r,\theta) &= e^{-j\frac{4\pi}{c}(f_c+m_n\Delta f)\left[r+\left(-\frac{N-1}{2}+n\right)d\sin\theta\right]} \\ &\approx e^{-j\frac{4\pi}{c}\left[f_c r+(n-\frac{N-1}{2})f_c d\sin\theta+m_n\Delta f r\right]}. \end{aligned} \tag{5}$$

The approximation in (5) holds if the phase error is less than $\pi/4$.

Then, in the single snapshot case, the noise-free received echo vector of one ideal unit target can be formulated by arranging all $b_n(r,\theta)$ in the order

$$\mathbf{b}(r,\theta) = [b_0(r,\theta), b_1(r,\theta), \ldots, b_{N-1}(r,\theta)]^T. \tag{6}$$

For multi-target, multi-snapshot and noisy scenario, if the range, azimuth and reflection amplitude of the ith target at the lth snapshot are r_i, θ_i and $\alpha_i(l)$ (the reflection amplitude can vary from snapshot to snapshot because of the fluctuation [2].), respectively, the echo vector of the lth snapshot is

$$\mathbf{r}(l) = \sum_{i=1}^{P} \alpha_i(l)\mathbf{b}(r_i,\theta_i) + \mathbf{n}(l), l = 1, 2, \ldots, L. \tag{7}$$

where P and L are the target number and snapshot number, and $\mathbf{n}(l)$ is the $N \times 1$ additive receiver noise vector.

3. BEAMPATTERN OF THE RFDA

The beampattern of the RFDA is the system response of the array beam that is formed at range r_1, azimuth θ_1 to a unit amplitude target at range r_2, azimuth θ_2 [4],

$$\begin{aligned} \beta(\{r_1,\theta_1\},\{r_2,\theta_2\}) &= \frac{<\mathbf{b}(r_1,\theta_1)\cdot\mathbf{b}(r_2,\theta_2)>}{\|\mathbf{b}(r_1,\theta_1)\|_2\|\mathbf{b}(r_2,\theta_2)\|_2} \\ &= \frac{1}{N}\sum_{n=0}^{N-1} b_n^*(r_1,\theta_1)b_n(r_2,\theta_2) \end{aligned} \tag{8}$$

where the asterisk denotes complex conjugation.

Substituting (5) into (8), the beampattern of the RFDA is

$$\begin{aligned} \beta(\{r_1,\theta_1\},\{r_2,\theta_2\}) &= \frac{1}{N}\sum_{n=0}^{N-1} e^{j\frac{4\pi}{c}(f_c+m_n\Delta f)(\Delta r+x_n\Delta\mu)} \\ &= \beta(\Delta r,\Delta\mu), \end{aligned} \tag{9}$$

where $\Delta r = r_1 - r_2$ and $\Delta\mu = \sin\theta_1 - \sin\theta_2$. According to the above derivation, the beampattern is determined by the difference in the range and azimuth sine and independent of the absolute range or azimuth. Letting $p = 2\Delta f\Delta r/c$, $q = 2df_c\Delta\mu/c$, and $\epsilon = \Delta f/f_c$, the beampattern can be further simplified as

$$\beta(p,q) = \frac{1}{N}e^{j2\pi\frac{p}{\epsilon}}\sum_{n=0}^{N-1} e^{j2\pi\left(n-\frac{N-1}{2}\right)q}e^{j2\pi m_n p}. \tag{10}$$

For the traditional FDA with linearly shifted carrier frequencies (LFDA), the beampattern $\beta(p,q)_{\text{LFDA}}$ can be achieved by alternating m_n with $n-(N-1)/2$ in (10).

$$\beta(p,q)_{\text{LFDA}} = \frac{1}{N}e^{j2\pi\frac{p}{\epsilon}}\sum_{n=0}^{N-1} e^{j2\pi(p-q)\left(n-\frac{N-1}{2}\right)}. \tag{11}$$

Fig. 2 compares the beampatterns of LFDA (Fig. 2(a)) and RFDA (Fig. 2(b)). The beampattern of the LFDA has high sidelobe ridges, which implies that the range and azimuth are coupled and the indication of target location is ambiguous. However, the beampattern of the RFDA is thumbtack-like,

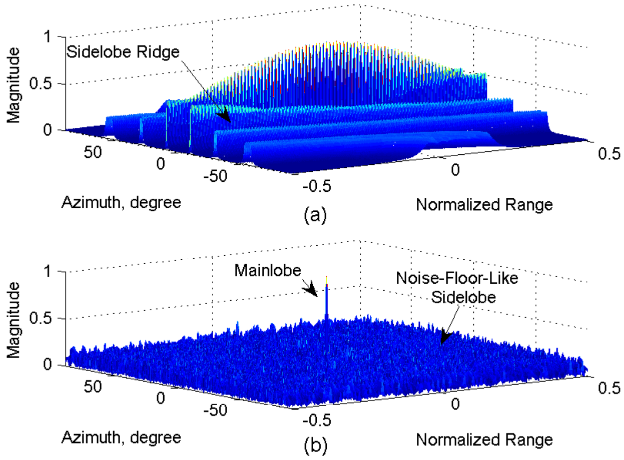

Fig. 2. Comparison of beampatterns. (a) LFDA; (b) RFDA.

and the peak is located where $p = 0$ and $q = 0$, which implies that the range and azimuth have successfully been decoupled and the target location can be uniquely and correctly indicated.

In Fig. 2(b), we can also find that the beampattern of RFDA has noise like sidelobe pedestals. Actually, the beampattern can be regarded as a random process with respect to p and q, and we have the following theorem,

Theorem 1 *If the antenna number N is sufficiently large, $\beta(p,q)$ is asymptoticly complex Gaussian distributed, whose mean $\bar{\beta}(p,q)$ and covariance matrix $\mathbf{M}(p,q)$ are*

$$\bar{\beta}(p,q) = E\left\{\beta(p,q)\right\} = \frac{1}{N} S_a^N(q)\Phi(p) \begin{bmatrix} \cos\alpha \\ \sin\alpha \end{bmatrix}, \quad (12)$$

$$\begin{aligned} \mathbf{M}(p,q) &= E\left\{[\beta(p,q) - \bar{\beta}(p,q)][\beta(p,q) - \bar{\beta}(p,q)]^T\right\} \\ &= \begin{bmatrix} \sigma_r^2 \cos^2\alpha + \sigma_i^2 \sin^2\alpha & \sin\alpha\cos\alpha(\sigma_r^2 - \sigma_i^2) \\ \sin\alpha\cos\alpha(\sigma_r^2 - \sigma_i^2) & \sigma_r^2 \sin^2\alpha + \sigma_i^2\cos^2\alpha \end{bmatrix} \end{aligned} \quad (13)$$

where $\alpha = 2\pi p/\epsilon$, $S_a^N(x) = \sin(N\pi x)/\sin(\pi x)$, $\Phi(x)$ is the characteristic function of $g(m_n)$, and

$$\sigma_r^2 = \frac{1}{2N}\left[1 - \Phi^2(p) - \frac{S_a^N(2q)}{N}\left(\Phi^2(p) - \Phi(2p)\right)\right]$$

$$\sigma_i^2 = \frac{1}{2N}\left[1 - \Phi^2(p) + \frac{S_a^N(2q)}{N}\left(\Phi^2(p) - \Phi(2p)\right)\right]$$

Furthermore, we can derive Proposition 1 for the sidelobe's magnitude.

Proposition 1 *For azimuth difference $q = \frac{1}{2N}$, the complementary cumulative distribution function of sidelobe's magnitude at $\{p, q\}$ satisfies*

$$Pr\{|\beta(p,q)| > r\} = Q_1\left(\frac{a}{\tau}, \frac{r}{\tau}\right) \quad (14)$$

where $Q_1(x,y)$ is the first-order Marcum Q-function,

$$Q_1(x,y) = \int_b^\infty t e^{-\frac{t^2+x^2}{2}} I_0(xt)dt$$

and $a = \frac{1}{N}|S_a^N(q)\Phi(p)|$, $\tau = \sqrt{\frac{1}{2N}(1-\Phi^2(p))}$.

The proof of Theorem 1 and Proposition 1 is mainly inspired by the Lyapunov Central Theorem (LCT) [10]. Details can be found in our full-length journal paper.

4. COMPRESSIVE SENSING FOR RANGE AND AZIMUTH INDICATION

In the RFDA, the thumbtack-like mainlobe indicates that the range and azimuth are uncoupled. However, in the multi-target scenario, the noise-floor-like sidelobes may cause the large target(s) to mask the weak target(s). In this paper, we adopt sparse recovery algorithms for compressive sensing to solve this problem.

The un-aliased range and azimuth extent are uniformly divided into P and Q grids. (For the aliasing problem in the FDA, the reader can refer to [5, 6] for more information.) Thus, there are PQ range-azimuth pairs $\{r_i, \theta_i\}$, where $i = 1, 2, \ldots, PQ$ in the un-aliased range and azimuth extent.

Define a $PQ \times 1$ vector $\mathbf{x}(l)$, whose ith entry is the complex reflection amplitude of the target at $\{r_i, \theta_i\}$ in the lth snapshot. The observing matrix $\mathbf{\Phi}$ is $N \times PQ$. The ith column of $\mathbf{\Phi}$ is determined by (5) and (6), where r and θ in (6) correspond to the range-azimuth pair $\{r_i, \theta_i\}$. Then, in the single-snapshot case (termed the Single Measurement Vector (SMV) scenario in the compressive sensing realm), the echo can be rewritten in a matrix form

$$\mathbf{r}(l) = \mathbf{\Phi}\mathbf{x}(l) + \mathbf{n} \quad (15)$$

where $\mathbf{n}$ is the receiver noise vector. If there are $L > 1$ snapshots, the echoes can be formed as a Multiple Measure Vector (MMV) scenario,

$$\mathbf{R} = \mathbf{\Phi}\mathbf{X} + \mathbf{N}, \quad (16)$$

where $\mathbf{R} = [\mathbf{r}(1), \mathbf{r}(1), \ldots, \mathbf{r}(L)]$, $\mathbf{X} = [\mathbf{x}(1), \mathbf{x}(1), \ldots, \mathbf{x}(L)]$, and $\mathbf{N}$ is the receiver noise matrix.

The sparse recovery algorithms estimate $\mathbf{x}$ or $\mathbf{X}$ by exploring its sparsity. A number of sparse recovery algorithms can achieve the most "sparse" solution of (15) or (16) with acceptable measurement errors. For the SMV scenario, the sparsest estimate of $\mathbf{x}(l)$ is

$$\min \|\mathbf{x}(l)\|_0, \text{ subject to } \|\mathbf{r}(l) - \mathbf{\Phi}\mathbf{x}(l)\|_2 \leq \sigma_l \quad (17)$$

where $\|\cdot\|_0$ is the number of non-zero entries.

For the MMV scenario, we select $\|\cdot\|_{2,0}$ (the number of row vectors with non-zero l_2 norms) to maintain the consistency of the targets' locations in all snapshots. The estimate of $\mathbf{X}$ is

$$\min \|\mathbf{X}\|_{2,0}, \text{ subject to } \|\mathbf{R} - \mathbf{\Phi}\mathbf{X}\|_F \leq \sigma_L \quad (18)$$

where $\|\cdot\|_F$ is the Frobenius norm. In (17) and (18), σ_l and σ_L are the error tolerances determined by the noise power.

In compressive sensing, the correct recovery can be guaranteed with high probability if the observing matrix $\mathbf{\Phi}$ has a small mutual coherence [9]. The mutual coherence is defined as the maximum normalized inner product of different columns of the observing matrix. Comparing this definition with (8), the mutual coherence is equal to the highest sidelobe in the beampattern. Fig. 2 shows that the highest sidelobe level of the RFDA is substantially lower than that of the LFDA. This property indicates that the RFDA is suitable for compressive sensing.

In this paper, the Subspace Pursuit (SP) [11], FOCUSS [12], and their MMV extensions (Generalized Subspace Pursuit (GSP) [13] and M-FOCUSS [14]) are adopted to recover the targets in both the SMV and MMV scenarios. The demonstration and performance comparison are provided in the next section.

5. NUMERICAL RESULTS

Simulations are conducted to evaluate the range and azimuth indication performance of the RFDA. In the simulation, m_n is discretely uniformly distributed as $g(m_n) = 1/M$, where M is a positive integer, and $m_n \in \{-\frac{M-1}{2}, -\frac{M-1}{2}+1, \ldots, \frac{M-1}{2}\}$. In this case, the total bandwidth of the CFDA is $(M-1)\Delta f$. The other system parameters are as follows: $f_c = 3$GHz, $N = 128$, $M = 128$, $\Delta f = 1$MHz, $d = 0.05$m.

The first simulation gives an example of target indication. There are three targets at different ranges and azimuths ($r_1 = 10\text{m}, \theta_1 = -30^o$; $r_2 = 70\text{m}, \theta_2 = 5^o$; $r_3 = 120\text{m}, \theta_3 = 60^o$.). The magnitudes of Targets 1 and 2 are identical and 10 dB larger than that of Target 3. The SNR of Target 3 is 0 dB (measured at the input of each receiver). Only one snapshot is used. The beamforming result is shown in Fig. 3(a). The ranges and azimuths of Targets 1 and 2 are correctly indicated, but Target 3 is too weak compared with the first two and is covered by their sidelobes. However, in the sparse recovery result (Fig. 3(b), using the SP algorithm), all three targets are successfully detected, and the locations are correctly indicated.

The second simulation is performed to evaluate the detection performance of different sparse recovery algorithms. There are two targets with identical reflection amplitudes but different locations. The input SNR varies from -24 dB to 6 dB. Successful detection is defined as the coincidence of the estimated and true support sets. The successful detection rate for each SNR point is obtained using 1000 Monte-Carlo trials. Results are illustrated in Fig. 4. In the comparison between SMV and MMV, the detection performances of the MMV are better for both types of algorithms. In the comparison among recovery algorithm types, FOCUSS and M-FOCUSS outperform their subspace pursuit counterparts in both SMV and MMV scenarios.

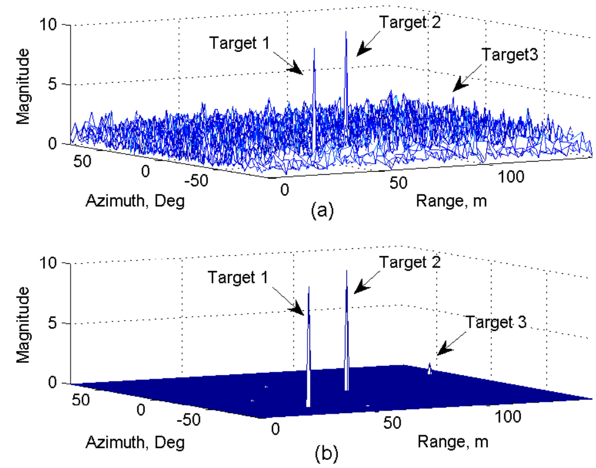

Fig. 3. Target range and velocity indication using the RFDA. (a) Beamforming result; (b) Sparse recovery result.

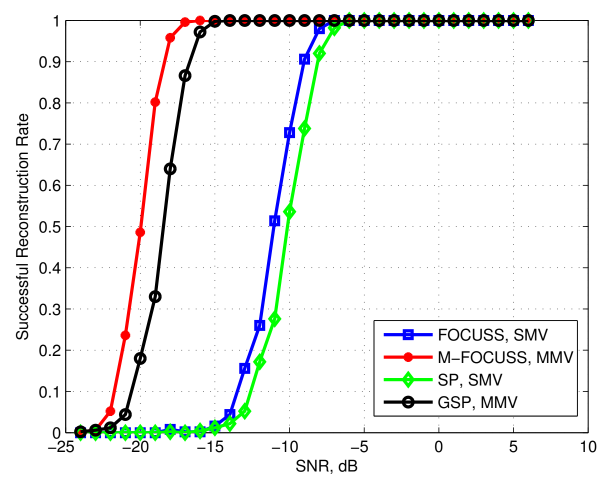

Fig. 4. Successful detection rates of different sparse recovery algorithms.

6. CONCLUSION

We propose a new array approach to indicate the range and azimuth of multiple targets without coupling. In the RFDA, each antenna has a narrow bandwidth, and the carrier frequency is randomly assigned across the array. The RFDA can be considered a random sparse sampling of target information in both the frequency and spatial domains; hence, it provides compressive sensing of both the range and azimuth simultaneously. With sparse recovery algorithms, the RFDA can detect targets with large magnitude differences and correctly indicate their locations. The performance of the RFDA is demonstrated with numerical results.

7. REFERENCES

[1] H. Van Trees, *Detection, estimation, and modulation theory, optimum array processing*, John Wiley & Sons, 2004.

[2] M. Skolnik, *Introduction to radar systems*, McGrow-Hill, 2001.

[3] T. Do-Hong and P. Russer, “Signal processing for wideband smart antenna array applications,” *IEEE Microwave Mag.*, vol. 5, no. 1, pp. 57–67, 2004.

[4] P. Antonik, M. Wicks, H. Griffiths, and C. Baker, “Frequency diverse array radars,” in *Proceeding of IEEE Radar Conference*, 2006, pp. 215 – 217.

[5] P. Sammartino, C. Baker, and H. Griffiths, “Frequency diverse mimo techniques for radar,” *IEEE Trans. AESS*, vol. 49, no. 1, pp. 201–222, 2013.

[6] J. Xu, G. Liao, S. Zhu, L. Huang, and H. So, “Joint range and angle estimation using mimo radar with frequency diverse array,” *IEEE Trans. SP*, vol. 63, no. 13, pp. 3396–3410, 2015.

[7] Y. Wang, W.-Q. Wang, H. Chen, and H. Shao, “Optimal frequency diverse subarray design with cram’errao lower bound minimization,” *IEEE AWP Letters*, vol. 2014, pp. 1188–1191, 2015.

[8] W.-Q. Wang and H. Shao, “Range-angle localization of targets by a double-pulse frequency diverse array radar,” *IEEE Journal STSP*, vol. 8, no. 1, pp. 106–114, 2014.

[9] Z. Ben-Haim, Y. Eldar, and M. Elad, “Coherence-based performance guarantees for estimating a sparse vector under random noise,” *IEEE Trans. SP*, vol. 58, no. 10, pp. 5030–5043, 2010.

[10] A. Kolmogorov and B. Gnedenko, *Limit distributions for sums of independent random variables*, Addison-Wesley, Cambridge, Mass, 1954.

[11] W. Dai and O. Milenkovic, “Subspace pursuit for compressive sensing signal reconstruction,” *IEEE Trans. IT*, vol. 55, no. 5, pp. 2230–2249, 2009.

[12] I. Gorodnitsky and B. Rao, “Sparse signal reconstruction from limited data using focuss: A re-weighted minimum norm algorithm,” *IEEE Trans. SP*, vol. 45, no. 3, pp. 600–616, 1997.

[13] J. Feng and C. Lee, “Generalized subspace pursuit for signal recovery from multiple-measurement vectors,” in *Proceeding of IEEE Wireless Communications and Networking Conference (WCNC)*, 2013, pp. 2874 – 2878.

[14] S. Cotter, B. Rao, K. Engan, and K. Kreutz-Delgado, “Sparse solutions to linear inverse problems with multiple measurement vectors,” *IEEE Trans. SP*, vol. 53, no. 7, pp. 2477–2488, 2005.